JOURNAL OF MAGNETIC RESONANCE **131,** 17–24 (1998)
ARTICLE NO. MN971340

Optically Detected Electron Spin Echo Envelope Modulation on a Photoexcited Triplet State in Zero Magnetic Field—A Comparison between the Zero-Field and High-Field Limits

V. Weis, K. Möbius, and T. Prisner*,[1]

*Institut für Experimentalphysik, Freie Universität Berlin, Arnimallee 14, 14 195 Berlin, Germany; and *Institut für Physikalische und Theoretische Chemie, Johann Wolfgang Goethe Universität, Marie Curie Strasse 11, 60 439 Frankfurt/Main, Germany*

Received May 5, 1997; revised November 17, 1997

Electron spin echo envelope modulation (ESEEM) has been studied at zero and low magnetic fields ($B \leq 100$ G) by means of optically detected magnetic resonance. Qualitative differences of the ESEEM effect for an electronic triplet state ($S = 1$) under low-field and high-field conditions are observed and discussed. They are related to the different properties of the total spin angular momentum operator $\hat{S}$ and the hyperfine interaction at zero and high magnetic field. The novel method was applied to the photoexcited triplet state of acridine-d_9 in a fluorene-h_{10} matrix. An analysis of the observed nitrogen quadrupole splitting is done by a quantitative description of the ESEEM effect in zero field.

Key Words: **electron spin echo envelope modulation (ESEEM); zero-field; optically detected magnetic resonance (ODMR); photoexcited triplet state; pulsed EPR.**

I. INTRODUCTION

An electron spin echo is a burst of microwave radiation from a sample containing paramagnetic species after the application of two or more microwave pulses (*1, 2*). In solids the echo intensity often shows a periodic change as the time between the microwave pulses is increased. This effect is called electron spin echo envelope modulation (ESEEM) and is due to anisotropic nuclear hyperfine interaction (*1*).

Fourier transform of the modulated echo decay reveals the ESEEM frequencies (the same as in an ENDOR experiment) and therefore the eigenvalues of the nuclear Hamiltonian. Additionally the ESEEM amplitudes contain information about the eigenfunctions of the nuclear Hamiltonian. Usually ESEEM experiments are simulated with an adjustable set of hyperfine parameters. Measurements at different frequencies/magnetic field strengths increase the accuracy of the fits as additional constraints on the parameter set are imposed (*3, 4*). Since commercial pulsed EPR spectrometers normally operate at X-band frequencies (8–10 GHz), most of the studies have been performed at magnetic fields of about 3000 G.

At zero magnetic field, EPR on systems with $S \geq 1$ is possible because the magnetic dipolar interaction between the electrons lifts the degeneracy of the spin state. Whereas ESEEM at high magnetic field is a widely used tool for detecting nuclear transitions within an inhomogeneously broadened resonance line, only a few publications exist for the zero-/low-field limit. Hoffman (*5*) investigated non-Kramers doublets ($S = 2$) and Jeschke and Schweiger (*6*) studied an $S = 5/2$ system, both having zero-field-splitting energies corresponding to X-band frequencies.

In the case of a triplet state ($S = 1$), the zero-field splitting is described by

$$\hat{H}_{\mathrm{ZFS}} = D(\hat{S}_z^2 - \tfrac{1}{3}\hat{S}^2) + E(\hat{S}_x^2 - \hat{S}_y^2) \qquad [1]$$

with the ZFS parameters D and E. Van Oort and Glasbeek (*7*) performed ESEEM experiments on the triplet state of N–V centers in diamond in an external magnetic field below 200 G. They analyzed their measurements in the high-field approximation because of the zero-field parameter $E = 0$. In this case the electronic spin states are eigenstates of the $\hat{S}_z$ operator, as for the high-field limit.

Janes and Brenner (*8*) detected a modulation on the echo decay of the TCB Y-trap (1,2,4,5-tetrachlorobenzene) at zero field which was assigned to a chlorine quadrupole transition, while van't Hof and Schmidt (*9*) detected a modulation studying quinoline triplet states. However, no quantitative analysis for zero-field ESEEM has been published so far for an $S = 1$ system.

Here we will give a quantitative theoretical description of zero-field ESEEM experiments for a general triplet-state molecule ($S = 1$, $D \neq 0$, $E \neq 0$). We will describe in

[1] To whom correspondence should be addressed. E-mail: prisner@chemie.uni-frankfurt.de. Fax: 49-69-798-29404.

1090-7807/98 $25.00

detail the differences compared to high-field ESEEM and, moreover, show the differences between zero-field ESEEM of single crystals and powder samples. Furthermore we discuss which information can be extracted from zero-field and low-field measurements.

II. HIGH-FIELD THEORY OF ESEEM

Excellent studies have been published describing the ESEEM effect in the high-field case by using density matrix formalism (*1, 10, 11*). We will use the notation of Mims (*1, 12*) and Dikanov *et al.* (*11*), which gives an adequate description of the physics of the ESEEM experiment.

Here we want to review the results of the electron spin echo modulation analysis that are important in understanding the differences between high- and zero-field experiments. To get an insight into the determination of the ESEEM frequencies and the modulation depth we consider the $S = 1/2$, $I = 1/2$ problem with the Hamiltonian (*11*)

$$\hat{H} = (\omega - \omega_0)\hat{S}_z + \omega_I\hat{I}_z + A\hat{S}_z\hat{I}_z + B\hat{S}_z\hat{I}_x, \qquad [2]$$

written in the rotating frame. A and B represent the secular and nonsecular parts of the hyperfine interaction, ω_0 and ω_I represent the electron and nuclear Larmor frequencies, and ω represents the frequency of the microwave irradiation. Due to the anisotropic hyperfine interaction B, mixing of the nuclear wavefunctions within the electron spin manifolds m_S occurs. The Hamiltonian of Eq. [2] can be diagonalized by the unitary transformation $\hat{H}_{\text{diag}} = \exp(i\phi\hat{I}_y)\hat{H}\exp(-i\phi\hat{I}_y)$, where the angle ϕ is determined by $\tan(\phi) = Bm_S/(Am_S + \omega_I)$. The operator $\exp(i\phi\hat{I}_y)$ in the product base can be written as

$$\exp(i\phi\hat{I}_y) = \left[\begin{array}{c|c} M_\alpha & \\ \hline & M_\beta \end{array}\right] \begin{array}{l} |+\tfrac{1}{2},-\tfrac{1}{2}\rangle \\ |+\tfrac{1}{2},+\tfrac{1}{2}\rangle \\ |-\tfrac{1}{2},-\tfrac{1}{2}\rangle \\ |-\tfrac{1}{2},+\tfrac{1}{2}\rangle \end{array}. \qquad [3]$$

The matrix $M_\alpha(M_\beta)$ describes the mixing of the nuclear spin functions in the $\alpha(\beta)$ manifold (*1*). If $M_\alpha = M_\beta$, only allowed ($\Delta m_I = 0$) EPR transitions occur and no modulation is observed. In the case $M_\alpha \neq M_\beta$, the transition moment for ''allowed'' EPR transitions is decreased while a transition probability for ''forbidden'' transitions ($\Delta m_I = \pm 1$) occurs and, consequently, ESEEM is observable; i.e., $M_\alpha \neq M_\beta$ is the necessary condition for the observation of the ESEEM effect. The transition matrix element between the ith nuclear level in the α manifold and the jth level of the β manifold is given by

$$M_{ij} = (M_\alpha M_\beta^\dagger)_{ij}, \qquad [4]$$

where $M_\beta^\dagger$ is the adjoint matrix of M_β. A simple expression results for the two-pulse-echo amplitude $\epsilon(\tau)$:

$$\epsilon(\tau) = \sum_{ij,kl} M_{ik}M_{kj}^\dagger M_{jl}M_{li}^\dagger \exp(-i\omega_{ij}^\alpha\tau)\exp(-i\omega_{kl}^\beta\tau). \qquad [5]$$

The summation over i and j extends only over the nuclear levels of the α manifold, while the summation variables k and l are restricted to the β manifold.

The matrix M determines the amplitudes of the individual modulation frequencies. In the $I = 1/2$ case Eq. [5] can be written as (*1*)

$$\epsilon(\tau) = 1 + \frac{K}{2} \times \left[\cos(\omega_\alpha\tau) + \cos(\omega_\beta\tau) - \frac{1}{2}\cos[(\omega_\alpha + \omega_\beta)\tau] - \frac{1}{2}\cos[(\omega_\alpha - \omega_\beta)\tau] - 1\right] \qquad [6]$$

with $K = (\omega_I B/\omega_\alpha\omega_\beta)^2$, giving the modulation depth $K/2$ for the frequencies ω_α, ω_β and $K/4$ for the sum and difference frequencies $\omega_\alpha + \omega_\beta$, $\omega_\alpha - \omega_\beta$.

III. ESEEM IN LOW MAGNETIC FIELD

The previously presented theory is valid also for electronic triplet states ($S = 1$) as long as the electronic Zeeman energy exceeds the zero-field splitting ($\gamma_e B_0 \gg D$), and only one of the dipolar splitting transitions is driven for a given magnetic field value ($D \gg \omega_1$). If the modulation depth parameter K (see Eq. [6]) is plotted versus the external field B_0 the maximum modulation is observed at a field strength for which the nuclear Zeeman splitting ω_I equals the hyperfine frequency

$$\omega_I = \pm m_S A, \qquad [7]$$

where m_S is the quantum number of the electronic state. In other words, at this external field value B_0, the isotropic part of the hyperfine field at the position of the nucleus is canceled and the quantization of the nuclear spin functions along B_0 is no longer given. This effect is known as ''exact cancellation.'' Under these conditions the transition probabilities for *forbidden* and *allowed* EPR transitions are equal.

At magnetic field strengths for which the high-field limit case is not valid, Eq. [7] changes to

$$\omega_I = \langle S\rangle A, \qquad [8]$$

where $\langle S\rangle$ has replaced m_S. $\langle S\rangle$ is the expectation value of the total spin angular momentum operator $\hat{S}$ at the given magnetic field strength. For a triplet state, $\langle S\rangle$ depends not

only on the absolute value of the external magnetic field but also on its orientation relative to the zero-field splitting tensor axes. The dependence of $\langle S\rangle$ on the external magnetic field is described by (*13*)

$$|\langle S\rangle_i| = \cos(\theta_i) - \sin(\theta_i) \quad \text{for } B_0 \| i \qquad [9]$$

with $\tan(2\theta_x) = (D + E)/2g\mu_B B_0$, $\tan(2\theta_y) = (D - E)/2g\mu_B B_0$, and $\tan(2\theta_z) = -2E/2g\mu_B B_0$ for the external magnetic field parallel to the ZFS x, y, z axis (g is the electron g factor, μ_B the Bohr magneton). The general case for an arbitrary orientation of the external magnetic field does not lead to simple analytical expressions and is not considered further. Equation [9] clearly shows that $\langle S\rangle$ is a function of the orientation of $\mathbf{B}_0$ (for a given strength B_0). The magnitudes of $D + E$, $D - E$, and $-2E$ determine how strong B_0 must be so that the triplet can be described in the high-field limit ($|\langle S\rangle| \approx 1$).

Figure 1 shows a plot of Eq. [9] for two different triplet states. The dotted trace is calculated with the zero-field parameters D and E of the acridine triplet state ($D = 2.22$ GHz, $E = -0.26$ GHz), while the solid trace corresponds to a smaller E value ($D = 2.22$ GHz, $E = -0.026$ GHz). The triplet state with the small E value can be described in the high-field limit for an external magnetic field as low as $B_0 \approx 50$ G.

Due to Eq. [9], the hyperfine interaction $\hat{H}_{HF} = \langle \hat{S}\rangle A\hat{I}$ smoothly increases from second-order interaction at zero field to a first-order effect as the magnetic field is increased. As a result, low external magnetic field experiments can no longer be simulated by the high-field approximation theory reviewed in Section II, as both the ESEEM frequencies and the modulation depth parameters K are predicted incorrectly. Figure 2 shows a comparison between the exact calculations and the results for the high-field approximation for a triplet state ($D = 2.22$ GHz, $E = -0.26$ GHz) with one nucleus I $= 1/2$. The elements of the hyperfine tensor were taken as $A = 250$ kHz and $B = 10$ kHz. The dotted trace shows the exact cancellation at $B_0 = 165$ G in the high-field approximation, while the real maximum mixing of the nuclear spin functions occurs at $B_0 = 140$ G.

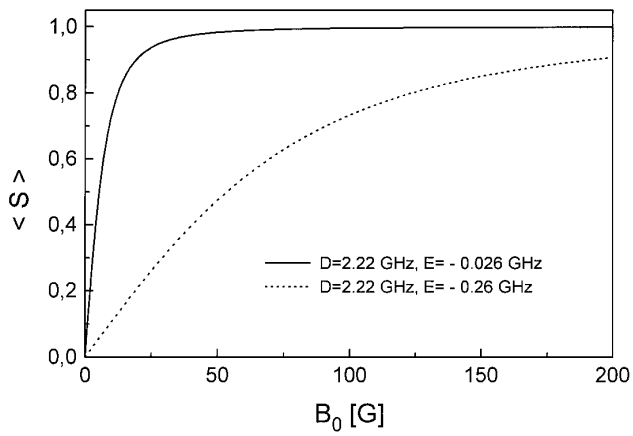

FIG. 1. Dependence of the expectation value $\langle S\rangle$ of a triplet state on the magnetic field strength for a static magnetic field along the z axis of the zero-field splitting tensor.

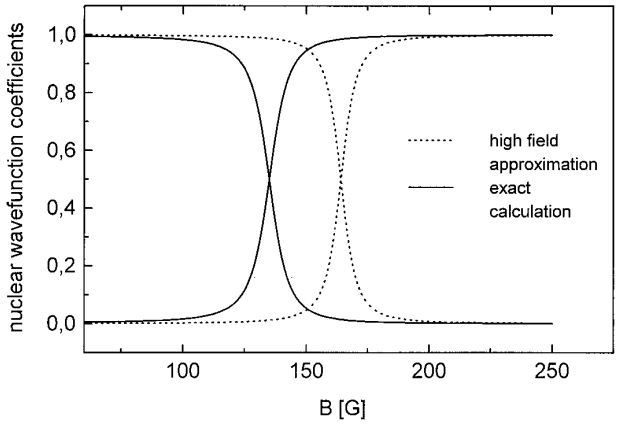

FIG. 2. Calculation of the cancellation condition for an $S = 1$, $I = 1/2$ system. The coefficients $|C_{+1/2}|^2$, $|C_{-1/2}|^2$ of the nuclear spin wavefunction ($\Psi_{nucl} = C_{+1/2}|\phi_{+1/2}\rangle + C_{-1/2}|\phi_{-1/2}\rangle$) in the electron manifold $M_S = +1$ are shown. The dotted line represents the mixing of the nuclear spin wavefunctions in the high-field approximation, whereas the solid line shows the exact calculation in the low-field case. The hyperfine tensor parameters A and B were taken as $A = 250$ kHz and $B = 10$ kHz (Eq. [2]).

Equations [7] and [8] give the conditions for maximum modulation depth. As long as the high-field conditions apply, only the nuclear Zeeman frequency ω_I is tuneable with the external magnetic field to fulfill the cancellation condition. In the low-field case two additional tuning possibilities of $\langle S\rangle$ are given (Eq. [8]):

- A change in the strength of the external magnetic field changes linearly the nuclear Zeeman splitting ω_I, while $\langle S\rangle$ has a dependence as described in Eq. [9].
- Rotating the zero-field splitting tensor relative to the external magnetic field affects $\langle S\rangle$, while the nuclear Zeeman frequency ω_I remains constant.

IV. ESEEM AT ZERO MAGNETIC FIELD

At zero external field the cancellation condition of Eq. [7] is no longer useful because the nuclear Zeeman term vanishes. Also the expectation value $\langle S\rangle$ is quenched in first order so that second-order perturbation theory has to be applied for the hyperfine interaction contributions. Before discussing this case in more detail some comments should be made concerning the hyperfine interaction at the various field conditions.

In the high-field limit the hyperfine interaction is often described with sufficient accuracy in terms of $\hat{S}_z A_{zi}\hat{I}_i$ with $i = x, y, z$. Only the nuclear spin wavefunctions are mixed and

TABLE 1
Spin Wavefunctions of the Electronic $|X\rangle$ and $|Z\rangle$ Triplet States Due to Second-Order Hyperfine Interaction

$$|Xy\rangle' = (1 - \tfrac{1}{2}\alpha^2)|Xy\rangle + \alpha|Yx\rangle$$
$$|Xx\rangle' = (1 - \tfrac{1}{2}\alpha^2)|Xx\rangle - \alpha|Yy\rangle$$
$$|Xz\rangle' = |Xz\rangle$$
$$|Zy\rangle' = |Zy\rangle$$
$$|Zx\rangle' = |Zx\rangle$$
$$|Zz\rangle' = |Zz\rangle$$

Note. The wavefunctions are written in the product base of the electron triplet and nuclear quadrupole wavefunctions. $|x\rangle$, $|y\rangle$, and $|z\rangle$ denote the nuclear quadrupole functions. Only the out-of-plane component of the hyperfine interaction, A_{zz}, has been considered. The mixing parameter α is explained in the text.

no mixing of the electron spin wavefunctions takes place. As a consequence the condition for the maximum ESEEM effect is fully determined by parameters of the nucleus, such as the nuclear Zeeman frequency ω_I and the hyperfine tensor.

In zero field, however, the hyperfine interaction acts in a different way. Hyperfine terms of the form $\hat{S}_x A_{xi}\hat{I}_i$, $\hat{S}_y A_{yi}\hat{I}_i$ must be considered as well as the $\hat{S}_z A_{zi}\hat{I}_i$ terms, thereby mixing the electron spin wavefunctions. This leads to a branching of the electronic transitions, necessary for the ESEEM effect.

As the nuclear Zeeman splitting is absent in zero field, the ESEEM modulations arise only from nuclear quadrupole and/or hyperfine interactions depending on the molecule under investigation. The mixing of the electronic spin functions at zero field is in the order of

$$\alpha = \sqrt{\frac{A^2}{(\Delta E)^2}} = \left|\frac{A}{\Delta E}\right|, \qquad [10]$$

where A represents the components of the hyperfine tensor and ΔE the energy difference between the electronic zero-field levels. α determines the branching ratio, as the transition probabilities $|\langle i|\gamma\mathbf{B}_1\mathbf{S}|j\rangle|^2$ for forbidden transitions are proportional to α^2. γ is the gyromagnetic ratio of the electron.

In order to observe ESEEM, both allowed and forbidden EPR transitions must be excited simultaneously by the magnetic field component of the microwave. In the high-field case this is done by the microwave magnetic field B_1 component perpendicular to the direction of the external magnetic field. Hence, any of the single-quantum EPR transitions in the triplet system is observable.

However, in the zero-field case the electron spin wavefunctions $|U\rangle$ $(U = X, Y, Z)$ are eigenfunctions of the ZFS Hamiltonian with the properties

$$\hat{S}_u|U\rangle = 0, \quad \hat{S}_x|Y\rangle = -\hat{S}_y|X\rangle = i|Z\rangle \quad \text{(cyclic)}, \qquad [11]$$

where $\hat{S}$ represents the total spin angular momentum operator. As a consequence a transition dipole moment γ $\langle X|\hat{S}_y|Z\rangle = i\gamma$ (cyclic) is present between any two of the triplet substates. It follows that the transition probability is proportional to

$$|\gamma\langle Z|\mathbf{B}_1\mathbf{S}|Y\rangle|^2 = (\gamma B_{1X})^2 \quad \text{(cyclic)}, \qquad [12]$$

where $\mathbf{B}_1$ is the amplitude of the magnetic component of the driving field $\mathbf{B}_1\cos(\omega t)$. The time dependence of the microwave term is removed by a unitary transformation to the interaction representation which is comparable to the rotating frame in the high-field description (*14*).

The electron spin wavefunctions become superpositions of the unperturbated triplet wavefunctions $|U\rangle$ $(U = X, Y, Z)$ as a result of second-order perturbation theory for the hyperfine interaction. It follows from Eq. [12] that all the magnetic components B_{1u} $(U = X, Y, Z)$ are needed to observe all transitions. Allowed and forbidden transitions are driven by different orthogonal components of the microwave magnetic field. This offers the possibility of increasing the magnetic field strength for forbidden transitions, while simultaneously decreasing the driving microwave component for the allowed transitions. Therefore, even an unfavorable branching ratio due to the hyperfine interaction can result in strong ESEEM modulations (see Section VI).

V. ZERO-FIELD ESEEM ON ACRIDINE-d_9

The ZF-ESEEM experiments described here were performed on acridine-d_9 guest molecules in a fluorene-h_{10} host

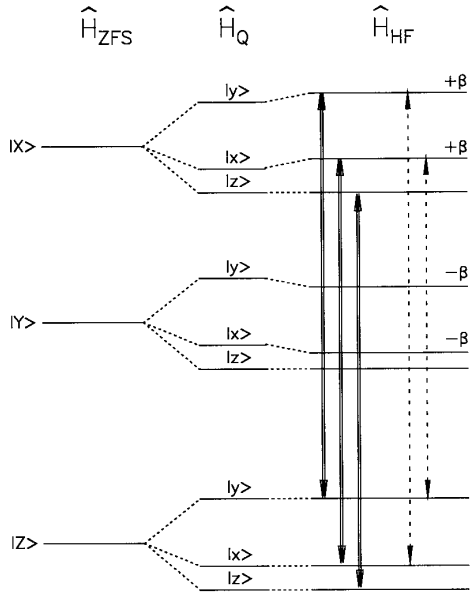

FIG. 3. Energy level diagram for the photoexcited triplet state of acridine and an $I = 1$ nuclear spin (nitrogen) considering only the A_{zz} hyperfine component. The system is described by the zero-field splitting $\hat{H}_{ZFS}$, the quadrupole interaction $\hat{H}_Q$, and the hyperfine interaction $\hat{H}_{HF}$. Allowed (solid line) and forbidden (dashed line) EPR transitions are shown.

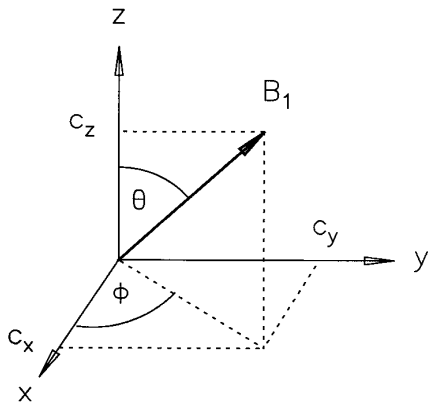

FIG. 4. Definition of the angles Φ, Θ in the axis system of the zero-field splitting tensor. The projections c_x, c_y, and c_z of the B_1 field are shown.

crystal. The photoexcited triplet state is detected, with the main hyperfine coupling arising from the nitrogen ^{14}N nucleus ($I = 1$). The spin Hamiltonian of this system can be expressed by

$$\hat{H} = \underbrace{D(\hat{S}_z^2 - 1/3\hat{S}^2) + E(\hat{S}_x^2 - \hat{S}_y^2)}_{\hat{H}_{\mathrm{ZFS}}} + \underbrace{Q[(3\hat{I}_z^2 - \hat{I}^2) + \eta(\hat{I}_x^2 - \hat{I}_y^2)]}_{\hat{H}_{\mathrm{Q}}} + \underbrace{\hat{S}A\hat{I}}_{\hat{H}_{\mathrm{HF}}}, \quad [13]$$

where $\hat{H}_{\mathrm{ZFS}}$ is the zero-field splitting Hamiltonian, $\hat{H}_{\mathrm{Q}}$ the quadrupole Hamiltonian of the ^{14}N nucleus, and $\hat{H}_{\mathrm{HF}}$ the hyperfine Hamiltonian. The parameters Q and η are the nuclear quadrupole coupling constant and the asymmetry parameter, respectively. The hyperfine interaction term cannot be simplified as in the high-field case. It contains all product terms of the form $\hat{S}_i A_{ij} \hat{I}_j$, making the entire Hamiltonian nondiagonal. The eigenenergies are calculated using second-order perturbation theory. Considering the symmetry of the molecule, the calculations are carried out with the following assumptions (*15, 16*):

- The principal axes systems of $\hat{H}_{\mathrm{ZFS}}$, $\hat{H}_{\mathrm{Q}}$, and $\hat{H}_{\mathrm{HF}}$ coincide.
- Only the out-of-plane component of the hyperfine interaction, A_{zz}, is considered for ^{14}N nuclei ($A_{zz} \gg A_{xx}, A_{yy}$). This assumption is justified because in second-order perturbation only A_{xx}^2, A_{yy}^2, and A_{zz}^2 appear so that the dominant contribution is due to A_{zz}.
- The hyperfine interaction of the deuterons and their quadrupole contributions are neglected ($A_D \ll A_{14_N}$, $Q_D \ll Q_{14_N}$).

As a result the energy levels are shifted in the order of β in energy, while the mixing of the wavefunctions due to hyperfine interaction is in the order of α (see Table 1), where α and β are given by

$$\alpha = \left| \frac{A_{zz}}{(E_x - E_y)} \right|, \quad \beta = \frac{A_{zz}^2}{(E_x - E_y)}. \quad [14]$$

E_i ($i = x, y, z$) are the eigenvalues of the zero-field splitting Hamiltonian $\hat{H}_{\mathrm{ZFS}}$. The calculated level scheme is shown in Fig. 3.

VI. CALCULATION OF THE ESEEM SIGNAL

The Hamiltonian describing the experiment in the zero-field basis is given by

$$\hat{H} = \underbrace{\hat{H}_{\mathrm{ZFS}} + \hat{H}_{\mathrm{Q}}}_{\text{diagonal}} + \underbrace{\hat{H}_{\mathrm{HF}}}_{\text{nondiagonal}} + \underbrace{(c_x\hat{S}_x + c_y\hat{S}_y + c_z\hat{S}_z)\gamma_e B_1 \cos(\omega_0 t)}_{\hat{H}_{\mathrm{MW}}}. \quad [15]$$

$\hat{H}_{\mathrm{MW}}$ represents the Hamiltonian due to microwave irradiation, where ω_0 is the frequency of the transition investigated. The coefficients c_x, c_y, and c_z are the projections of the microwave B_1 field onto the ZFS tensor axes x, y, and z, as shown in Fig. 4.

The ESEEM signal of Eq. [5] is fully determined when knowing the level scheme and the matrix M which contains all the information about the branching. M is easily calculated by

$$M = T\hat{H}_{\mathrm{MW}}T^{-1}, \quad [16]$$

where T represents a unitary transformation to diagonalize the Hamiltonian without the microwave term, i.e.,

$$\hat{H}_{\mathrm{diagonal}} = T[\hat{H}_{\mathrm{ZFS}} + \hat{H}_{\mathrm{Q}} + \hat{H}_{\mathrm{HF}}]T^{-1}. \quad [17]$$

Once M is calculated it is possible to determine the amplitudes of the ESEEM frequencies.

Again we want to emphasize that the amplitude of each observable ESEEM frequency is determined not only by the principal values of the given hyperfine interaction tensor within the molecule but also by its orientation relative to the direction of the microwave magnetic field. This aspect is a special property of the zero-field condition and does not appear in the high-field limit.

If ESEEM measurements are performed on powder samples, one must keep in mind that for each orientation of the molecule the modulation depth K of an individual ESEEM frequency varies, while its spectral position remains unchanged in the absence of an external magnetic field. Integra-

tion over the orientational dependence of K yields a reduction of the entire modulation depth. In the following a powder average for the acridine molecule will be considered. The modulation amplitude for the nuclear transition frequency ω_{ij}^{α} is proportional to

$$\sum_k |M_{ik}|^2 |M_{kj}|^2, \qquad [18]$$

where the index k runs over all the levels of the β manifold. For simplicity we consider only a four-level system in which allowed and forbidden transitions occur. This simplification holds also for our triplet system because the contributing levels for the ESEEM effect are only the $|Zx\rangle$, $|Zy\rangle$, $|Xx\rangle'$, and $|Xy\rangle'$ levels (Fig. 3 and Table 1). In accordance with Mims (*1*) we call the transition dipole moments for allowed and forbidden transitions v and u, respectively. In the high-field case the resulting modulation depth is $K = 4|u|^2|v|^2$.

In the zero-field case the transition dipole moments are scaled by the projections of the $\mathbf{B}_1$ field on the ZFS axes (c_x, c_y, c_z). Therefore, the modulation depth for the acridine $|Z\rangle - |X\rangle$ transition is given by

$$K_{zx} = 4|u|^2|v|^2 c_x^2 c_y^2. \qquad [19]$$

The powder case requires integration over all the molecular orientations relative to the B_1 direction. Equation [19] is rewritten by using the angles Φ, Θ, as defined in Fig. 4. The modulation depth $\overline{K_{zx}}$ after integration is

$$\overline{K_{zx}} = \frac{1}{2\pi^2}\int_0^{\pi} d\Theta \int_0^{2\pi} d\Phi K_{zx}(\Theta, \Phi) = [4|u|^2|v|^2]\frac{3}{64}. \qquad [20]$$

Compared to the maximum modulation depth $K_{zx}^{\max} = |u|^2|v|^2$, which occurs for $c_x = c_y = 1/\sqrt{2}$, the ''averaged'' depth is $\overline{K_{zx}} = 3/16K_{zx}^{\max}$.

VII. EXPERIMENTAL SETUP

A schematic representation of the experimental setup is shown in Fig. 5. The experiments were performed in pumped liquid helium in a bath cryostat (1.4 K). The sample was excited with the third harmonic (355 nm) of a pulsed Nd:YAG laser with pulse lengths of 12 ns. The phosphorescence of the sample is collected in a direction perpendicular to the light excitation and analyzed either by a photomultiplier or by an optical multichannel analyzer (OMA) in a gated mode. The microwave excitation can be achieved either by using a conventional slow-wave helix or by using a tuneable bridged loop–gap (BLG) resonator allowing also microwave detection (*17*). The microwave pulses are shaped

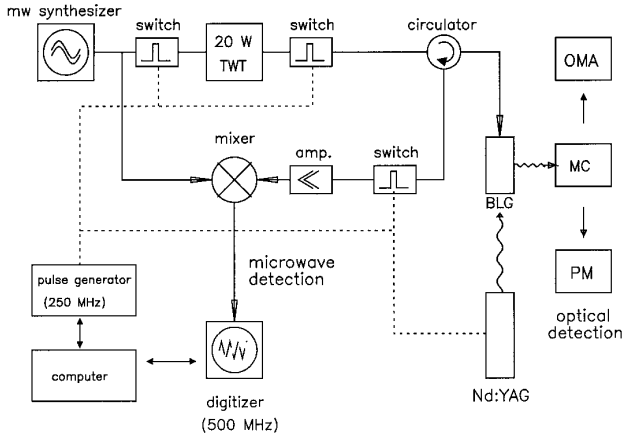

FIG. 5. Experimental setup for pulsed microwave ODMR experiments in zero/low magnetic field. TWT, traveling wave tube amplifier; MC, monochromator; PM, photomultiplier; OMA, optical multichannel analyzer; amp., GaAs low-noise amplifier; BLG, tuneable bridged loop–gap resonator (*17*).

at low microwave power (+10 dBm at the output of the microwave synthesizer) and then amplified by a 20-W TWT amplifier. The pulse lengths achieved for a π pulse are 300 ns for the helix and 45 ns for the BLG resonator. The master clock of the experiment used to trigger the laser as well as the OMA and all the microwave switches is a pulse generator with a time resolution of 4 ns.

The ESEEM measurements were performed with the following pulse sequence:

$$\underbrace{\text{laser pulse}-\tau_D-\pi/2-\tau-\pi}_{\text{excitation}}\ \underbrace{-\tau'-\pi/2}_{\text{preparation}}\ \underbrace{}_{\text{detection}}. \qquad [21]$$

The $\pi/2$ pulse at the time τ' after the π pulse is needed to enable optical detection of the electron spin echo (*14*). It transforms the optically silent echo signal at $\tau' = \tau$ into an optically detectable population difference. The net echo signal was recorded by subtracting the phosphorescence signal with $\tau' \neq \tau$ from the signal at $\tau' = \tau$.

The optical detection concept circumvents the problem of deadtime during the detection since the optical detection channel is not disturbed by the microwave excitation pulses. Echo signals can be recorded for τ values as small as 16 ns.

VIII. RESULTS AND DISCUSSION

Figure 6 shows an optically detected two-pulse ESEEM experiment of the $|X\rangle - |Z\rangle$ transition of acridine-d_9 in fluorene-h_{10} at zero magnetic field ($\nu \approx 2.478$ GHz). The echo decay was recorded by stepping the pulse spacing τ in steps of 36 ns up to $\tau = 3.6$ μs. The signal shown in Fig. 6 was filtered in order to eliminate the echo decay function.

The dominating line at 3 MHz is assigned to the $|x\rangle - |y\rangle$ ^{14}N quadrupole transition. A peak at 6 MHz with an amplitude ratio of 1:5 compared to the 3-MHz peak is assigned to a double-quantum transition. It is the sum of the $|x\rangle - |y\rangle$ quadrupole transitions of the electronic $|X\rangle$ and $|Z\rangle$ manifold. The amplitude ratio is in good agreement with the predicted value from calculations of the M matrix (1:6).

As expected, the modulation depth is strongly dependent on the sample position within the microwave helix. Changing the sample position changes the ratio c_x/c_y and therefore the branching ratio of the EPR transitions.

We investigated also the $|Y\rangle - |Z\rangle$ transition ($\nu \approx 1$ GHz) and detected the same ESEEM frequencies as for the $|X\rangle - |Z\rangle$ transition. The $|X\rangle - |Y\rangle$ transition, for which no branching and therefore no ESEEM is expected, could not be observed because of its low resonance frequency ($\nu \approx 0.5$ GHz).

The modulation depth was estimated to be $K \approx 0.3$ compared to the maximum echo amplitude. This strong modulation depth is created by a small mixing coefficient of the electronic spin wavefunctions of only $\alpha = 0.06$ (Table 1). In the high-field case a mixing of nuclear wavefunctions of the same amount would cause a modulation depth of only $K = 0.01$. This difference between high and zero field is due to the additional tuning possibility (c_x, c_y, c_z) in zero field.

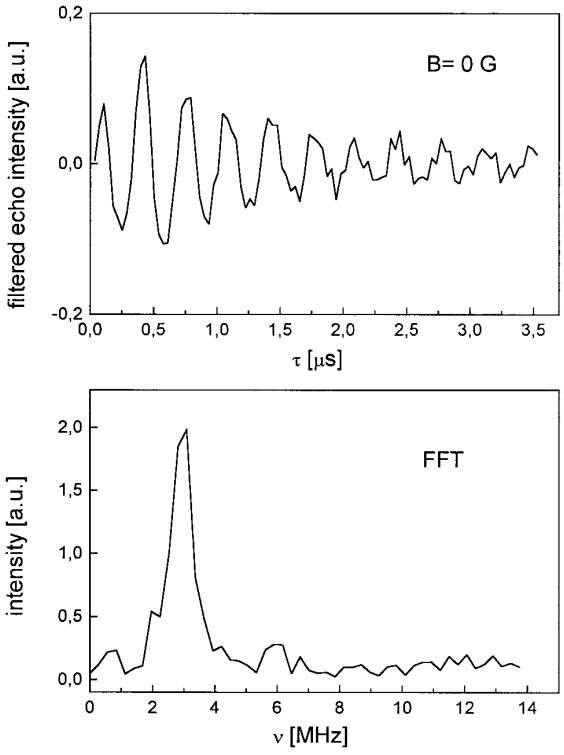

FIG. 6. Optically detected two-pulse ESEEM on the $|X\rangle - |Z\rangle$ transition of acridine-d_9 in fluorene-h_{10} at $T = 1.4$ K, $B = 0$ G and its Fourier transform. The echo decay was filtered in order to extract the modulation due to the ESEEM effect.

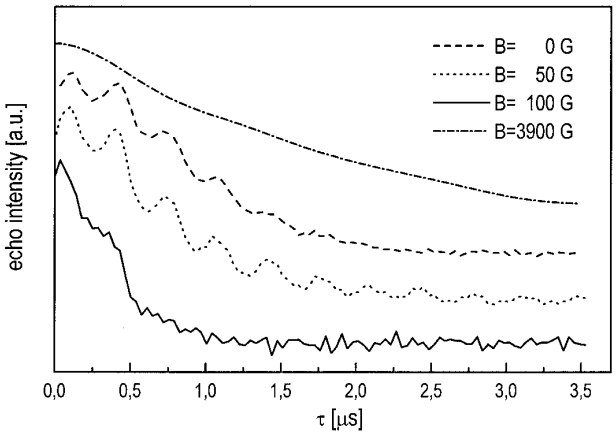

FIG. 7. Optically detected two-pulse echo decays on the $|X\rangle - |Z\rangle$ transition of acridine-d_9 in fluorene-h_{10} at $T = 1.4$ K at $B = 0$, 50, and 100 G with the magnetic field along the zero-field splitting x axis. The echo decay at $B = 3900$ G was recorded with conventional microwave detection. Its ESEEM modulation has been filtered in order to show the enhanced phase memory time compared to the zero- and low-field measurements.

An increase of the modulation depth is observed at $B = 50$ G (Fig. 7). Although the ratio c_x/c_y is identical to the zero-field situation, a change in the branching ratio takes place. For a detailed analysis the M matrix must be recalculated including the Zeeman term. At $B = 50$ G the calculation predicts an increase of the modulation depth for the magnetic field along x, while a decrease is expected for the magnetic field along the molecular y or z axis. This has been confirmed by our measurements. A reduction of the ESEEM amplitude has been observed in the $|Y\rangle - |Z\rangle$ transition with a magnetic field lying in the molecular y/z plane.

At about 100 G a shortening of the echo decay function is observed (Fig. 7). The nuclear Zeeman splitting of the matrix protons ($\omega_I \approx 420$ kHz) is comparable to the ^{14}N $|x\rangle - |z\rangle$ quadrupole transition in the electron $|Z\rangle$ manifold. This energy level crossing leads to an enhanced nuclear flip-flop rate and therefore reduces the phase memory time. This interpretation is strongly supported by ESEEM measurements at high magnetic field ($B = 3900$ G) at which an increase of the phase memory time is detected (Fig. 7).

A polycrystalline sample was used for the powder measurements. Its conventional frequency-swept ODMR spectrum at zero field was identical to the single-crystal spectrum. The ESEEM measurement of the powder sample is shown in Fig. 8. The modulation depth is strongly reduced, as is expected from the calculations (Section VI). Also the signal-to-noise is reduced due to the fact that the microwave pulse lengths are optimum only for a narrow range of molecular orientations. For the remaining orientations the pulse lengths used are not optimized, and therefore only a reduced echo intensity is observed.

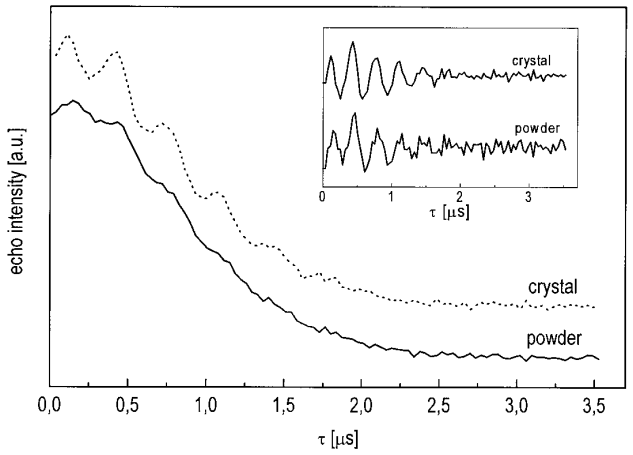

FIG. 8. Optically detected two-pulse ESEEM on a polycrystalline sample of acridine-d_9 in fluorene-h_{10} and its comparison to the crystal measurement. The inset shows the normalized ESEEM modulations.

IX. CONCLUSIONS

ESEEM in the absence of a magnetic field turns out to be a complementary method to nuclear quadrupole resonance (NQR) for determining quadrupole and/or hyperfine couplings which are not resolved in the zero-field EPR spectrum. Only small mixing coefficients α of the electronic spin wavefunctions are needed to make ESEEM in zero field possible. This is due to the special situation in zero field which allows one to increase the transition probability for forbidden transitions. According to $\alpha = |A/\Delta E|$, small zero-field splitting parameters are favorable for observing ESEEM in zero field.

The frequency resolution of the ESEEM spectrum is determined by the echo decay time. It can be improved by applying a stimulated echo sequence. Also quadrupole couplings smaller than those for ^{14}N may then become observable. Furthermore, the method can be applied to optically nonactive molecules if microwave detection is employed using a tuneable microwave resonator for zero-field transition frequencies (*17*).

ESEEM measurements in the low magnetic field range ($|\langle\hat{S}\rangle| < 1$) may be used to separate quadrupole and hyperfine interactions. Including a Zeeman term along the ZFS axis i, the nuclear Hamiltonian—which determines the observable ESEEM frequencies—is given by

$$\hat{H} = \hat{H}_Q + \sum_{k \neq i} \langle\hat{S}\rangle_i A_{ik} \hat{I}_k + [\langle\hat{S}\rangle_i A_{ii} + \gamma_I B_0] \hat{I}_i . \quad [22]$$

ESEEM frequencies measured for a fixed orientation of $\mathbf{B}_0$ for various field strengths lead to a set of equations for the hyperfine tensor parameters A_{ik}. $\langle\hat{S}\rangle_i$ is fixed when the ZFS parameters D and E are known. In the case of a powder sample, integration of the orientational dependence of $\langle\hat{S}\rangle_i$ must be done, which reduces the observable ESEEM modulation depth.

ACKNOWLEDGMENTS

We are grateful to H. Zimmermann (MPI Heidelberg) for synthesizing the acridine-doped fluorene crystals and to Professor H. M. Vieth (Freie Universität Berlin) for the donation of some acridine mixed crystals. We thank Professor H. van Willigen (University of Massachusetts, Boston) for the opportunity to perform the X-band measurements.

This work was supported by the Deutsche Forschungsgemeinschaft (SFB 337).

REFERENCES

1. W. B. Mims, *Phys. Rev. B* **5,** 2409–2419 (1972).
2. K. M. Salikhov, A. G. Semenov, and Yu. D. Tsetkov, ''Electron Spin Echoes and Their Application,'' Nauk, Novosibirsk (1976).
3. M. Romanelli, V. Kurshev, and L. Kevan, *Appl. Magn. Reson.* **7,** 427–441 (1994).
4. D. J. Singel, *in* ''Advanced EPR: Applications in Biology and Biochemistry'' (A. J. Hoff, Ed.), pp. 119–133, Elsevier, Amsterdam/New York (1989).
5. B. M. Hoffman, *J. Phys. Chem.* **98,** 11657–11665 (1994).
6. G. Jeschke and A. Schweiger, *Chem. Phys. Lett.* **259,** 531–537 (1996).
7. E. van Oort and M. Glasbeek, *Chem. Phys.* **143,** 131–140 (1990).
8. S. M. Janes and H. C. Brenner, *Chem. Phys. Lett.* **95,** 23–29 (1983).
9. C. A. van't Hof and J. Schmidt, *Mol. Phys.* **38,** 309–320 (1978).
10. M. K. Bowman and R. J. Massoth, *in* ''Electronic Magnetic Resonance of the Solid State'' (J. A. Weil, M. K. Bowman, J. R. Morton, and K. F. Preston, Eds.), pp. 99–110, Canadian Society for Chemistry, Ottawa, Canada (1987).
11. S. A. Dikanov, A. A. Shubin, and V. N. Parmon, *J. Magn. Reson.* **42,** 474–487 (1981).
12. W. B. Mims, *Phys. Rev. B* **6,** 3543–3545 (1972).
13. A. Carrington and A. D. McLachlan, ''Introduction to Magnetic Resonance,'' pp. 118–121, Harper & Row, New York (1967).
14. W. G. Breiland, H. C. Brenner, and C. B. Harris, *J. Chem. Phys.* **62,** 3458–3475 (1975).
15. C. B. Harris and M. J. Buckley, *in* ''Advances in NQR'' (J. A. Smith, Ed.), Vol. 2, pp. 15–70, Heyden, London (1975).
16. K. P. Dinse and C. J. Winscom, *J. Chem. Phys.* **68,** 1337–1343 (1978).
17. V. Weis, W. Mittelbach, J. Claus, K. Möbius, and T. Prisner *Rev. Sci. Instrum.* **68,** 1980 (1997).